Texture evolution during Isothermal compression process of Ti-22Al-25Nb alloy in B2 phase region

Haoyuan Ma[a,b], Weidong Zeng[a,b], Xiongxiong Gao[a,b], Youping Zheng[a,b]
a. State Key Laboratory of Solidification Processing, School of Materials Science and Engineering, Northwestern Polytechnical University, Xi'an, 710072, China
b. Defense Technoloies Innovation Center of precision forging and ring rolling, School of Materials Science and Engineering, Northwestern Polytechnical University, Xi'an, 710072, China

Abstract

In the present work, the hot deformation behavior, dynamic recovery, dynamic recrystallization and texture evolution of Ti-22Al-25Nb alloy on the conditions of 1100°C with four different thickness reductions (35%, 50%, 65% and 80%) are investigated by isothermal compression testing on Gleeble-3500 thermo-mechanical simulator. The strain rate is 0.1mm/s^{-1}. Subsequently, metallographic observation and EBSD analysis are carried out. The results show that during the hot deformation, the dynamic recovery (DRV) and dynamic recrystallization (DRX) strongly affect the microstructure and texture evolution. It is observed that with the strain increasing, the intensity of η_{bcc}-fiber increases firstly (crystallographic fiber axis <100> parallel to the compression direction). When the thickness reduction reaches to 80%, the intensity of <001> pole becomes stronger expectedly. Whereas the η_{bcc}-fiber transform into cube components ({100} <001>) unexpectedly. In addition, as the strain increases through 35%-80%, the fraction of large misorientation grain boundaries and fraction of DRX grains gradually increase due to continuous recrystallization. The evolution mechanism of grain orientations and texture during the DRX process will be discussed.

Keywords
Isothermal compression, B2 phase, texture, dynamic recrystallization, Ti-22Al-25Nb

Introduction

Ti_2AlNb based alloys have gained great popularity in the aerospace industry [1-5]. This new low-density high-temperature intermetallic compound material has higher high-temperature strength and high-temperature creep resistance than general titanium alloys. And it has higher plasticity, toughness, and deformability than Ti-Al-based alloys. At the same time, it has low linear expansion coefficient, non-magnetic property and high flame retardancy [4-6]. It can be used at 650 °C ~ 750 °C for a long time or at a higher temperature for a short time. The remarkable characteristics make Ti_2AlNb-based alloys a high-temperature structural material with great potential in the aerospace industry, and a new light-weight material is most likely to replace some high-density nickel-based superalloys [3, 7, 8]. Generally, titanium alloys exhibit flow softening when they are deformed in the β single-phase region. Dynamic recovery and dynamic recrystallization are the main softening mechanisms. Ding et al. [19] studied the microstructure evolution of Ti-6Al-4V alloy during deformation in the β-phase region. It is found that

due to the high stacking fault energy (SFE) of β-phase, dynamic recrystallization is relatively unlikely to occur during the deformation process, and dynamic recovery is the main softening mechanism. At high temperatures, atoms have a higher rate of diffusion. And due to the higher stacking fault energy of Ti_2AlNb based alloy, the dislocations in a slip system or between different slip systems are prone to slip, climb, and cross-slip. A large amount of dislocation motion can reduce the accumulated deformation energy. The strong recovery reduces the energy used to drive recrystallization, so recrystallization in the beta single phase region is more difficult to occur. Scholars Wu. Yang et al. [11] analyzed the microstructure evolution and recrystallization of Ti-22Al-25Nb based alloys. Studies have found that dynamic recovery and dynamic recrystallization occur in Ti_2AlNb-based alloys during hot deformation, and which could make the intensity of texture weaker.

Meanwhile, it is well known that texture has an important influence on the properties of materials. The texture evolution during hot deformation is affected by the restoration behavior. The scholars H.C Kou et al. and M. Hasegawa et al. [14, 15] pointed out that the texture evolution during the hot deformation is also a complicated process because the hot deformation can enhance the texture while the restoration behavior will change the intensity of texture. But most scholars believe that recrystallization will weaken the texture. In the current experiment, it is observed a different result. It was observed that the type of texture changed, and the orientation of the grains does not become random after recrystallization. Research on the relation between restoration and texture evolution of Ti_2AlNb based alloys is still not much.

In this paper, the thermal simulation compression test and EBSD analysis reveal the relation between restoration process and texture evolution of Ti-22Al-25Nb alloy during hot deformation. The reason for the influence of dynamic recovery and dynamic recrystallization on texture evolution is also speculated. It should be noted that there is no strict dividing line between GDRX (geometric dynamic recrystallization), CDRX (continuous dynamic recrystallization), and DDRX (discontinuous dynamic recrystallization). As of now, this study is still very limited, so there is no specific distinguish from these three types of dynamic recrystallization. A deeper mechanism remains to be further studied.

Experiments

The material tested in this study is a test bar, which is Ti_2AlNb based alloy, with a nominal composition of Ti-22Al-25Nb as the research material. The measured true composition is shown in Table 1. The density of present alloy is 5.35g/cm^3. The transus of the B2+O two-phase zone to the B2+α2+O three-phase zone of this alloy is 975 °C, which is measured by differential thermal analysis (DTA). The transus of the B2+α2+O three-phase zone to the B2+α2 two-phase zone is 1010 °C. The transus of the B2+α2 two-phase zone to the B2 unidirectional zone is 1060 °C. The bar repeatedly forged by the B2 single-phase zone, the B2+O two-phase zone, and the B2+α2+O three-phase zone. The cooling method for each step of forging is air cooling.

Table 1 Chemical composition of Ti-22Al-25Nb alloy (at%)

Ti	Al	Nb	O	N	H
Bal.	22.2	25.7	0.0430	0.0052	0.0009

In order to ensure the uniformity of the structure of each sample as much as possible, as shown in Figure 1, the hot-compression samples are cut by a wire-electrode cutting at the fixed radius of the bar. The axial direction of the sample is parallel to the axial direction of the bar. The surface of cut samples

are machined to remove the wire-electrode cutting influence layer, and the final specification of the sample is Ø8×12 (mm).

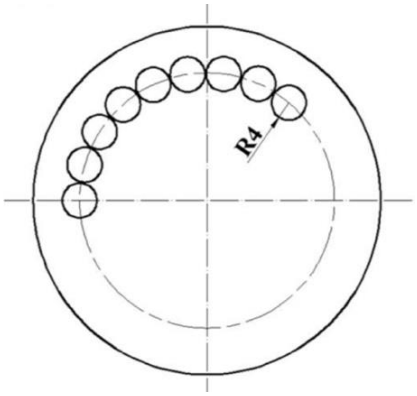

Fig.1 Positions of thermal compression samples on the bar.

The isothermal compression test is conducted on a Gleeble-3500 thermal-mechanical simulator at constant temperature of 1100°C. Before the compression testing, the samples are solution-treated at 1100°C (B2 phase region) for 30 min followed by water quenching to obtain a single B2 microstructure firstly. Then, they are heated to the target temperature with a rate of 10 °C s^{-1} and hold for 5 min before the commencement of deformation. Four different thickness reductions of samples are 35%, 50%, 65%, and 80% respectively. In addition, once the compression deformation is completed, the samples were quenched in water immediately to obtain the deformed microstructures. Subsequently, these four samples are observed by Olympus GX71 optical microscope and analyzed by HKL-EBSD detector which is equipped in TESCAN NOVA3 scanning electron microscope (SEM). The EBSD scanned regions and optical observed regions are in a longitudinal section at a half of radius. As shown by the red dot in Figure 2. The EBSD test data is processed by HKL Channel5 software. Simulation of 2D stress distributions were performed by Deform 11.0. The simulation result shows that the equivalent strain (ES) of scanned regions in the figure are about 0.48, 0.79, 1.21, and 1.79.

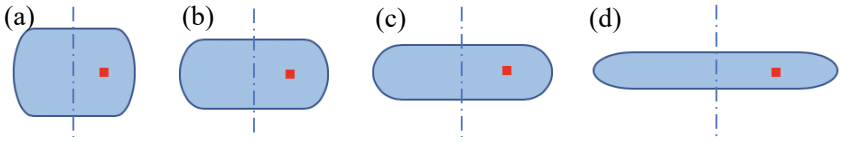

Fig.2 EBSD scan position of four thermal compression samples. (a) 35%, (b) 50%, (c) 65%, (d) 80%

Results and discussion

Evolution of microstructure and texture

The metallograph of four different thickness reductions is shown in Fig.3. From figure (a) to figure (d), with the thickness reductions increase in turn, grains are gradually flattened. In terms of the section, the B2 grains become elongated. In space, the B2 crystal grains are gradually crushed from an equiaxed state into an oblate shape. As shown in Fig.3(a), 3(b) and 3(c), with the compression increases, band structures are formed near the grain boundaries. The original B2 grain boundary changes from smooth to jagged. Such band structures are generally considered to be the deformed character. However, in Fig.3 (d) with 80% thickness reduction, the band structures become faint. And a necklace-like smaller equiaxed grains appeared in the original B2 grain boundary.

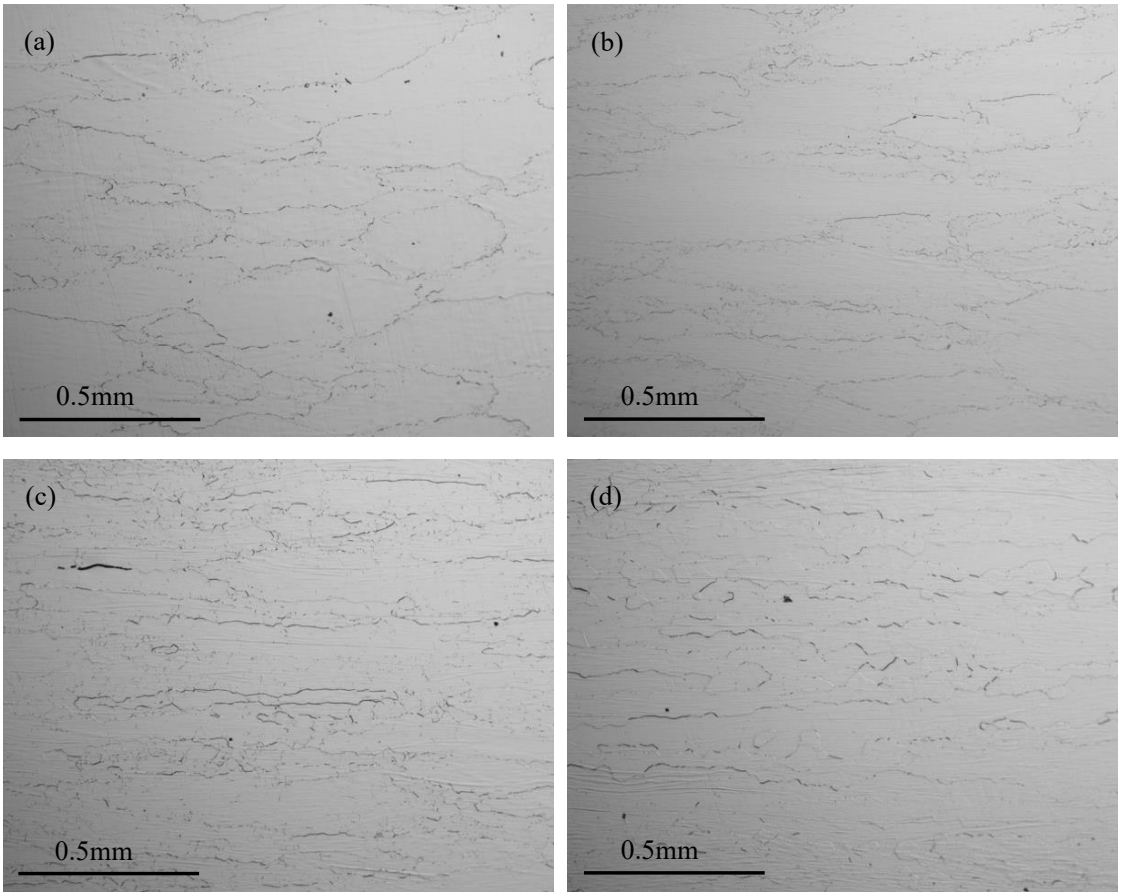

Fig.3 Metallograph of the samples deformed at 0.1s^{-1} and 1100^{o}C with different height reductions: (a) 35%, (b) 50%, (c) 65% and (d) 80%.

In the IPF coloring maps Fig.4, the grain boundaries with misorientations >15° are defined as high angle grain boundaries (HAGBs, white line) and those with misorientations between 2° and 15° are defined as low angle grain boundaries (LAGBs, black line). Consistent with previously observed phenomena, the density of black lines is gradually increasing with deformation of grains. It can be considered that these black lines represent the subgrain boundaries caused by the deformation. It looks like the maximum of the density of subgrain boundaries appears in the 65% thickness reduction of the four samples. When the thickness reduction reaches to 80%, we can see that a necklace structure appears in the original grain boundary. Generally, such features mark the emergence of DRX (dynamic recrystallization). From Fig. 4 and Fig. 5, it is indicated that the recrystallization is difficult to produce without enough deformation.

As shown in Fig.7, four pole figures (PF) is corresponding four thickness reductions respectively. Fig.7(a) is corresponding to thickness reduction of 35% which shows a relative random orientation. From Fig.7(a) to (c), the feature of fiber texture become more and more obvious. They are <111> fiber which axis <111> parallel to the compression direction and η_{bcc}-fiber which axis <100> parallel to the compression direction. But when the thickness reduction reaches to 80%, the feature of cube components ({100} <001>) appears and the previous fiber texture gets weaker. During the thickness reduction from 35% to 80%, the intensity of <100> pole continues to increase from 7.67 of Fig.7(a) to 18.57 of Fig.7(d).

It should be noted that the intensity of fiber texture changed when the thickness reduction is 50% to 80%. At 50% thickness reduction, the maximum value of the intensity of <111> pole is about to 12.45, and the intensity of pole <100> is about to 10. While, at the thickness reduction of 65%, maximum intensity value of pole <100> is 13.76. The intensity of pole <111> drops to 9 at the same time. However,

when the thickness reduction reaches 80%, the intensity of the <100> pole further increases to 18.57. The pole <111> intensity is weaker, about 5.

The relation between restoration behavior and texture

The recrystallization fraction maps are shown in Fig.5(a) to (d). The regions colored by blue, yellow and red represent recrystallized, substructured and deformed regions. Generally, the recrystallized regions are regions with the misorientations among adjacent probe points is less than 2° [20]. And the misorientation of 15° is the critical value to distinguish substructured regions and deformed regions. It is obvious that the fraction of recrystallization is increasing with the increasing of thickness reduction.

The fractions of each structure are shown in the Fig.6. The fraction of recrystallization hardly changes during the thickness reduction from 35% to 50% (equivalent strain0.48 and 0.79). However, the substrctured regions and the fraction of DRV regions increase during this process. It is means that the dynamic recovery (DRV) is the dominated phenomenon when the equivalent strain less than 0.79 (50% thickness reduction). The equivalent strain values for the EBSD detective regions of four samples are mentioned in the experimental section. When the thickness reduction reaches to 65% (equivalent strain 1.21), the substrctured regions still keep increasing. Moreover, the fraction of recrystallized regions has been significantly improved as well. It is indicated that dynamic recrystallization (DRX) could occur at equivalent strain of 1.21. The DRV and DRX both present a considerable volume at the current deformation conditions (DRV is about 33%, and DRX is about 23%.).

When the thickness reduction continues to increase to 80% (equivalent strain 1.79), the fraction of substrctured regions goes down to 20%, and the fraction of recrystallized regions goes up to about 34%. Interestingly, at the same time, the type of texture has changed from η_{bcc}-fiber to cube components. There may some relationships between these two phenomena. The formation of cube components may relative to the dynamic recrystallization.

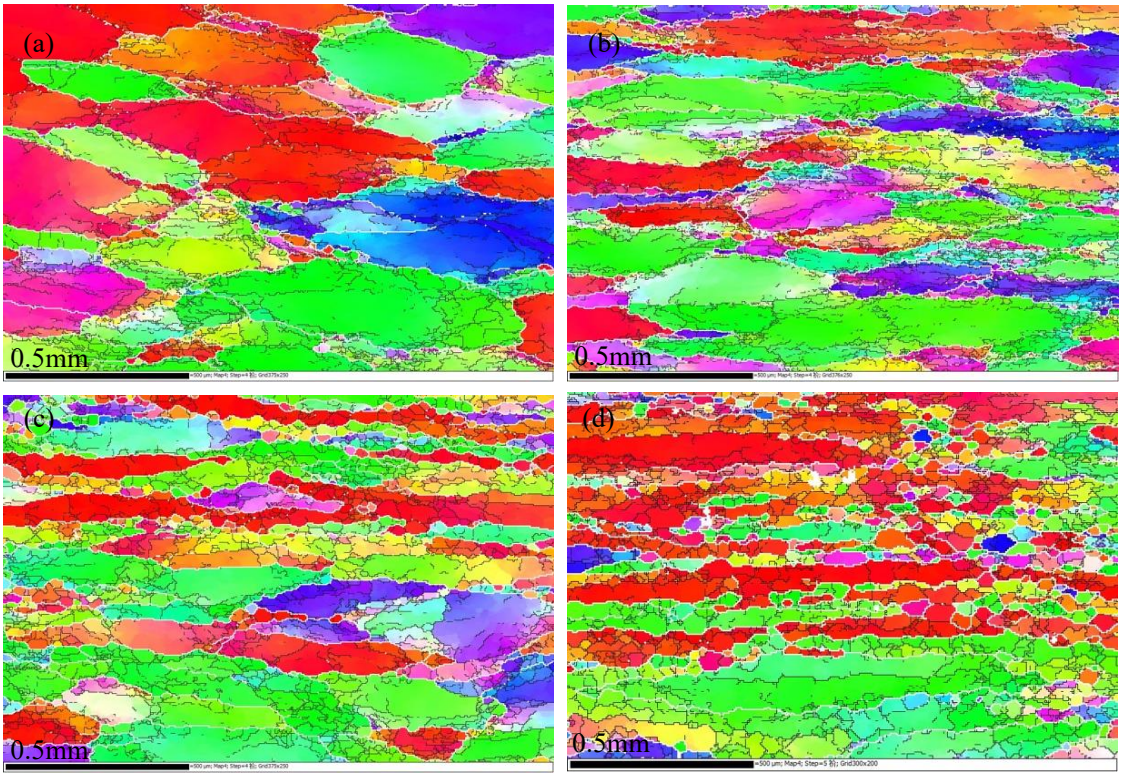

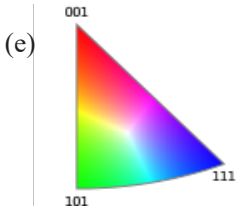

Fig.4 IPF(Y) coloring orientation maps mix misorientation of grain boundary maps of four samples deformed at 0.1s^{-1} and 1100^{o}C with different height reductions: (a) 35%, (b) 50%, (c) 65% and (d) 80% (e) IPF coloring legend.

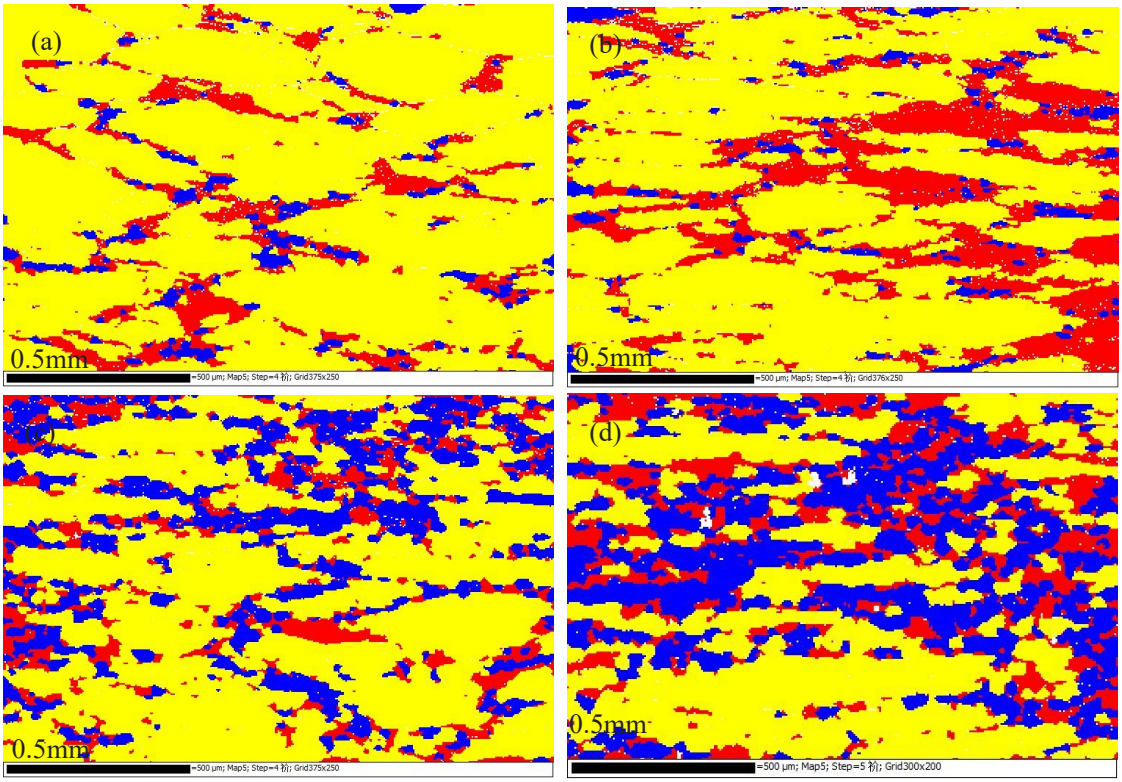

Fig.5 Recrystallization fraction maps in microstructures deformed at 0.1s^{-1} with height reduction of (a) 35%, (b) 50%, (c) 65% and (d) 80%.

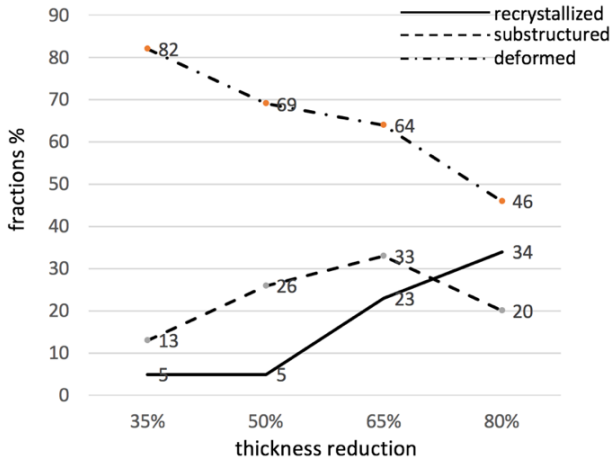

Fig.6 Recrystallized, substructured and deformed grains fraction of different thickness reductions.

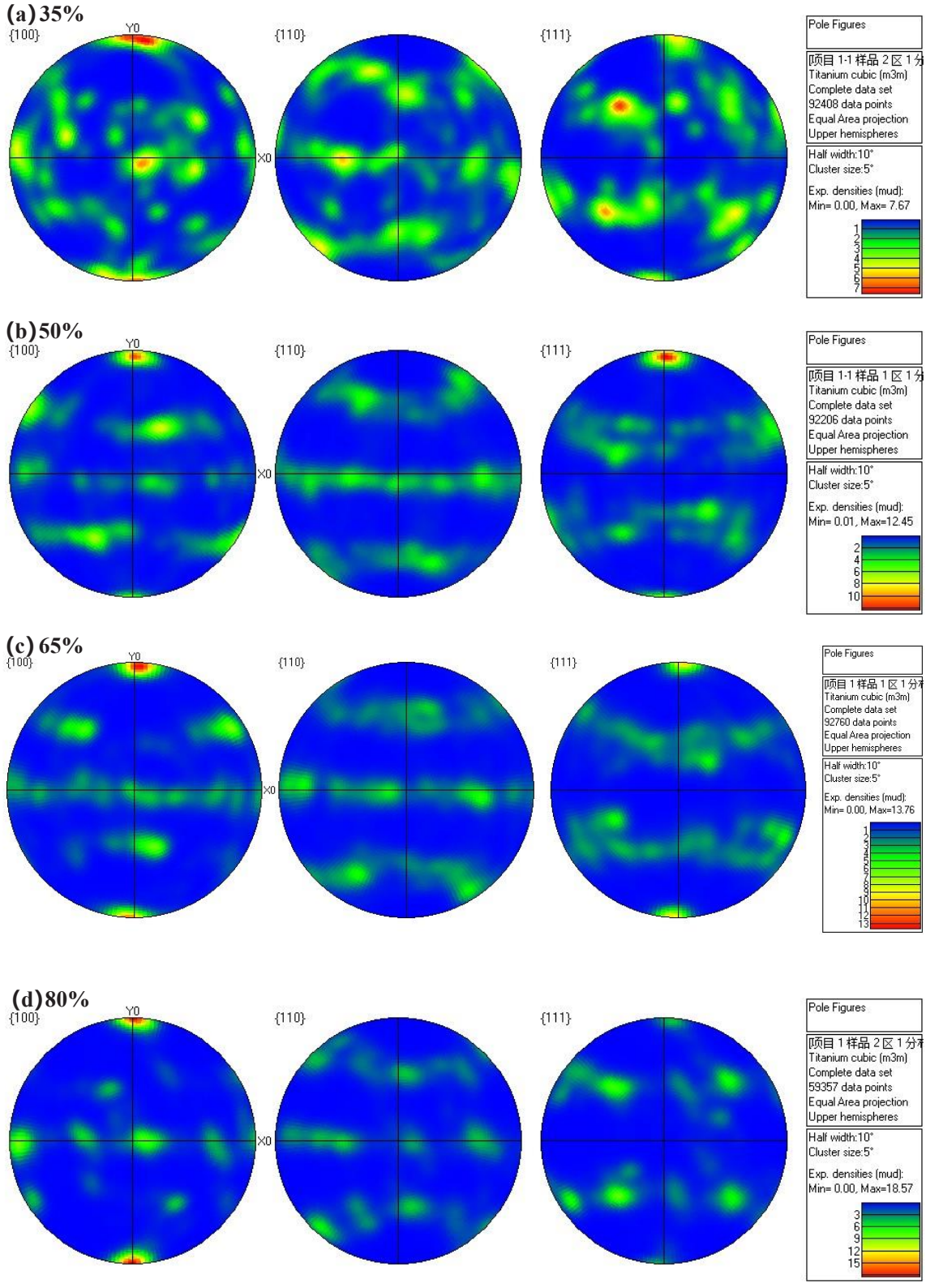

Fig.7 Pole figures (PF) of (a) 35%, (b) 50%, (c) 65% and (d) 80%.

The most obvious difference between recovery and recrystallization is whether the presence of grain boundary migrates or not. At high temperatures, during recovery process, edge dislocations can obtain enough energy to climb and cross-slip. The dislocation walls can be formed by dislocation climb and cross-slip, which can significantly reduce the elastic distortion energy of the dislocation [20]. A dislocation wall (small angle grain boundary) arranges perpendicularly to the slip plane which produces a polygonal structure. The result from this process is called substructures or subgrain boundaries. For an original

grain, the DRV process may disperse the original orientation to several contiguous orientations. In this way, the increasing amount of subgrain boundaries may result in a part of grain rotates. There is no migration of grain boundaries in recovery process. With the strain increases, the amount and fraction of subgrain boundaries will increase continuously until the DRX occurs. The characteristic of fiber texture is the orientation has one axis fixed and the perpendicular directions could rotate randomly. In the macroscopic view, the partial rotations of different grains are random. This point maybe one of the reasons to form the fiber textures.

A large misorientation of interface can migrate and it usually has a high migration rate [21]. From Fig.6, the fraction of high angle grain boundaries (HAB) increases a lot with the increasing strain. Migration and coalescence of HABs could decrease the fraction and amount of subgrain boundaries. It means the misorientation no longer changes continuously during the coalescence peocess. Eventually, at macro level, the texture components are produced which instead of the fiber texture [16].

Conclusions

With the strain increases, DRV and DRX are dominant in turn. When thickness reduction from 35%(ES=0.48) to 50%(ES=0.79), DRV is the main phenomenon. When thickness reduction from 50% to 65%(ES=1.21), the DRV and DRX both are the dominant phenomenon. When thickness reduction reaches to 80%(ES=1.79), the DRX becomes the main restoration mechanism with a lower fraction of DRV. The texture type changed, at the same time, as the main restoration mechanism changed. Different restoration process results in different texture types. DRV process more likely leads to produce fiber texture. While the occurrence of DRX lead to produce cube components instead of fiber texture. The formation of cube components is possible attributed to the dynamic recrystallization. More detailed analysis is looking forward to further studies.

References

[1] G. Lütjering, JC Williams Titanium. Springer-Verlag, Heidelberg 2007.
[2] Leyens, Christoph, and M. Peters. Titanium and Titanium Alloys: Fundamentals and Applications. Titanium and Titanium Alloys. 2003.
[3] Kumpfert, J. Advanced Engineering Materials, 3(2001), 851-864.
[4] W. Chen, J.W. Li, L. Xu, B. Lu. Advanced Materials & Processes, 2014, 172 (2): 23-27.
[5] J. Shen, A.H.Feng Acta Metallurgica Sinica, 2013, 49 (11): 1286-1294.
[6] J.W. Zang, S.Q. Li, X.B. Liang Acta Metallurgica Sinica, 2010, 20 (S1): 336-340.
[7] A.H. Feng, B.B. Li, J. Shen. Journal of Materials and Metallurgy, 2011, 10 (1): 30-38.
[8] Y.F. Si, L.H. MengAerospace Materials & Technology, 2006, 36 (3): 10-13.
[9] Y.G. Zhang, Y.F. Chen, G.L. Chen Intermetallic compound structural material. Beijing: national defense industry press, 2001: 28-91.
[10] D. Banerjeea, J.C. Williams. Acta Materialia, 2013, 61(3):844-879.
[11] Wu Y, Kou H, Wu Z, et al. Journal of Alloys and Compounds, 2018, 749:844-852.
[12] D. Banerjee, A.K. Gogia, T.K. Nandy, V.A. Joshi. Acta Metallurgica, 1988, 36 (4): 871-882.
[13] C.J. Boehlert, B.S. Majumdar, V. Seetharaman, D.B. Miracle. Metallurgical & Materials Transactions A, 1999, 30 (9): 2305-2323.
[14] H.C. Kou, Y. Chen, B. Tang, et al., Journal of Alloys and Compounds. 603 (2014) 23-27.

[15] M. Hasegawa, M. Yamamoto, H. Fukutomi, Acta Materialia 51 (2003) 3939-3950.

[16] Askeland, Fulay D R, Wright P P, et al. The Science And Engineering Of Materials. Tsinghua university press, 2005.

[17] C.J. Boehlert. Metallurgical & Materials Transactions A, 2001, 32 (8):1977-1988.

[18] K. Muraleedharan, T.K. Nandy, D. Banerjee, S. Lele. Metallurgical Transactions A, 1992, 23 (2): 417-431.

[19] Ding R, Guo Z X, Wilson A. Materials Science & Engineering A, 2002, 327(2):233-245.

[20] Huang K, Logé, R.E. Materials & Design, 2016, 111:548-574.

[21] Doherty R D, Hughes D A , Humphreys F J , et al. Materials Science and Engineering A, 1997, 238(2):219-274.